World Academy of Science, Engineering and Technology
International Journal of Materials and Metallurgical Engineering
Vol:13, No:2, 2019

Effect of Zinc Oxide on Characteristics of Active Flux TIG Welds of 1050 Aluminum Plates

H. Fazlinejad, A. Halvaee

***Abstract*—**In this study, characteristics of ATIG welds using ZnO flux on aluminum was investigated and compared with TIG welds. Autogenously AC-ATIG bead on plate welding was applied on Al1050 plate with a coating of ZnO as the flux. Different levels of welding current and flux layer thickness was considered to study the effect of heat input and flux quantity on ATIG welds and was compared with those of TIG welds. Geometrical investigation of the weld cross sections revealed that penetration depth of the ATIG welds with ZnO flux, was increased up to 2 times in some samples compared to the TIG welds. Optical metallographic and Scanning Electron Microscopy (SEM) observations revealed similar microstructures in TIG and ATIG welds. Composition of the ATIG welds slag was also analyzed using X-ray diffraction. In both TIG and ATIG samples, the lowest values of microhardness were observed in the HAZ.

***Keywords*—**ATIG, active flux, weld penetration, Al 1050, ZnO.

I. Introduction

INCREASING weld penetration depth can be obtained by increasing power density in a process. Processes like Electron Beam Welding (EBW) and Laser Beam Welding (LBW) are known to be effective in increasing energy density, while being costly [1]-[9]. Tungsten Inert Gas (TIG) welding is widely known as a relatively low-cost process, requiring simple and light equipment, with acceptable quality; but limited in use due to its low production rate resulting from shallow penetration. In order to increase this penetration, efforts have been made on modifying the TIG process. Increasing penetration depth by coating the surface with a thin layer of flux is called Active Flux TIG (ATIG); and was first introduced in 1960's in PATON Welding Institute in Ukraine. Studies on ATIG welds were also carried out in other centers, resulting in application of this method to industry [10]-[12].

Implementing active flux in welding was first applied in TIG process. Although the majority of research works in this area were conducted on GTAW process [10]-[28], there are also some studies on other welding processes such as GMAW [29], EBW [30], LBW [2], [31], SAW [32] , and PAW [33].

Pure aluminum, due to its high flexibility and corrosion resistant properties, has been applied to a wide range of industrial uses, including packaging, low strength corrosion resistant vessels and tanks, cladding, and roofing. This alloy also demonstrates high weldability [34].

H. Fazlinejad is with the Material Engineering Dept., Science & Research Branch, Azad University of Tehran, Ashrafi Esfahani Exp., Tehran, Iran (corresponding author, phone: +98-26-34209953; fax: +98-21-22137506, e-mail: hfazlinejad@gmail.com).

A. Halvaee is with the Material Engineering Dept., Science & Research Branch, AZAD University of Tehran, Ashrafi Esfahani Exp., Tehran, Iran.

Zinc oxide is an inorganic refractory compound with decomposition temperature of 1975°C, which is widely used in industries such as rubber and plastic, paint, lubricant, ointment, and food manufacturing. ZnO is a semiconductor with good transparency, high electron mobility, and high thermal conductivity properties. Application of this compound as active flux in welding has been studied by previous researchers. Dhandha et al. [35] study on stainless steel demonstrated a significant penetration depth increase using ZnO flux. Huang et al. [36] study revealed that by the use of a mixture of MnO2 and ZnO, the mechanical characteristics were also improved in addition to the penetration depth increase. Choudhary et al. [37] research demonstrated a minor depth penetration improve on Stainless Steel 304 base metal using ZnO flux. Kumar and Sathiya [38] reported that by using ZnO single flux in ATIG welding on Incoloy 800 H base metal, penetration depth decreased. Increasing penetration depth by applying ZnO flux has been reported by some other researchers [39], [40].

In some of the other studies, instead of coating the whole surface with flux, a gap of a few millimeters width at the center of the weld line left non-coated in order to establish a more stable arc transition, and the effects was studied. This process was named as FBTIG (Flux Bounded TIG) [26], [16], [13].

Previous studies are mainly performed on stainless steel as the base metal [10]-[12], [17], [19]-[21], [23]-[28], [31], [35]-[37], [40]. The possible reason is that TIG is a common process in stainless steel welding. There are also some research works on base metals such as aluminum [13], [14], [39], [16], Incoloy [38], Mg [22], and Ti [15], [18], [41] alloys.

Sire and Marya [13] investigated the effect of SiO_2 as the flux on AL5086 base metal, and demonstrated that relative penetration (D_{ATIG}/D_{TIG}) ratio was improved up to 2 times. Huang et al. [14] studied the effect of SiO_2 and AF305 mixed flux on Al 3003 base metal and investigated the mechanism. The D_{ATIG}/D_{TIG} ratio was increased up to 3 times. Jayakrishnan et al. [16] applied SiO_2 on pure aluminum with FBTIG process and studied the effect of flux gap and particle size.

Penetration depth as a geometrical characteristic of weld is affected by weld pool flow direction [42], [43]. This flow in general is derived by the electromagnetic force known as Lorents, buoyancy force, the shear stress acting on the pool surface by the arc plasma, and the shear stress induced by the surface tension gradient at the weld pool surface or Marangoni convection [44], [42]. The reversing of Marangoni convection

which introduced by Heiple [45] is the main suggested mechanism to explain penetration depth increase with active flux. In absence of surface activating agents, the surface tension decreases by rising liquid temperature. Since the weld pool temperature is higher at the arc center, the melt flows outward as a result of higher surface tension at the edges. This flow transfers more heat to the edges and tends to form a wide and shallow weld pool [42], [43], [46]. In presence of surface-active agents, surface tension increases by rising liquid temperature, thus the melt flows on the surface from the edges to the center and then to the depth. This effect occurs within a specific range of activating agent concentration; and for higher or lower concentration values, penetration increase is not observed [44], [24], [28].

Another mechanism suggested to explain penetration depth increase with active flux, is arc constriction and consequently increasing the arc power density at the center of weld [10], [13], [18], [26]. Electron absorption by elements derived from flux decomposition in the outer space of the arc plasma, has been suggested to explain arc constriction [10], [13]. Another suggested explanation is flux resistance against arc transition and consequently reducing anode spot size [3], [26]. Some of the other researchers, referred to presence of both of the mechanisms of reverse Marangoni convection and arc constriction together in a welding process [44], [47], [48].

In this study, ZnO is applied as flux on pure aluminum base metal to investigate whether it can act as an active flux in Aluminum welding. The effect of current and flux quantity on geometrical characteristics of Aluminum ATIG welds, particularly penetration depth is studied. In addition, microstructure and hardness of welds cross section is compared with those of TIG welds.

II. Experimental Method

In this study, 8 mm thick cold rolled commercial pure Aluminum EN-AW 1050A(H14) was selected as the base metal and ZnO as the flux. The Chemical composition of the base metal is presented in Table I. The purity of commercial ZnO powder was over 98%.

TABLE I
CHEMICAL COMPOSITION OF THE BASE METAL

Element	Al	Si	Fe	…
wt.%	99.61	0.073	0.231	< 0.02

Plates of 8 mm thickness were cut into 100x100 mm^2 samples using shear cutting machine. Two variable parameters were selected. The first was "heat input" that was varied in three steps by changing the current; and the second parameter was "flux quantity" that was controlled by "flux layer thickness" in 3 levels. In addition, 3 samples without flux (TIG weld samples) were welded as a reference at each heat input value. Finally, 12 samples including nine coated and three references were prepared.

In order to remove physical and chemical contaminants, surface of samples was cleaned first by steel wire brush and then by acetone. Flux powder of ZnO with particle sizes of less than 30 μm was spattered on the plates' surfaces by vibrating a 30 μm mesh screen from a 100-mm distance. In order to obtain sufficient adhesion and bonding between the flux particles and the plates, a volatile liquid like acetone was sprayed before and after spattering every layer. Similar method for coating the plates with flux has been reported by Lu et al. [24]. In many other studies, for coating the samples with the flux, a paste-like mixture of powder in a liquid (mostly acetone) had been applied on the surface with a brush [1], [3], [10], [11], [14], [22]-[24]. This method for applying the flux may result is a non-homogenous coating [26]. Ruckert et al. compared two solvents of distilled water and acetone regarding particles size and distribution [26].

Equal flux coated areas of 40x80mm^2 were obtained on all the plates using a template film. Flux layer thickness was calculated based on the plates' weight increase after application of the powder. Considering the flux powder density of D_{ZnO}=5.606 gr/cm^3 and the surface area of 32 cm^2, the required weight increases to obtain the flux thicknesses of 30, 60, and 90 μm were calculated as 0.538, 1.076, and 1.614 gr and were measured with a precise scale

In this study, three levels of 30, 60 and 90 μm were considered for flux thickness. The heat input was first controlled by current intensity; and then arc length and travel speed were slightly adjusted to obtain a smooth weld on test plates (Table II). Initial experiments illustrated that pre-heating is required to avoid formation of porosity.

TABLE II
EXPERIMENTS PARAMETERS VALUES

Parameter	Value	Unit
Material	1050A Aluminum	
Plate dimension	100 * 100	**mm**
Weld length	70	**mm**
Welding Current	105-140-175	**A**
Welding Speed	400-450-550	**mm/min**
Arc length	1-2-2.5	**mm**
Electrode– Tip angle	EWP-Ø2.4mm-30°	
Gas Flow rate	12 – Argon	**lit/min**
Preheat temp.	150	**℃**

Bead on plate weld with no filler metal was applied. The arc length and travel speed were controlled by fixing the torch head on a mobile carrier travelling on a rail. Arc initiation on the flux coated aluminum was difficult, so the welding was started on the non-coated area of the plates and after formation of the weld pool the torch was moved towards the coated area. Principal adjusted parameters were listed in Table II.

Test samples were cut out by sawing, according to the pattern schematically shown in Fig. 1. Visual inspection and measurement result recording were performed before test samples were cut out.

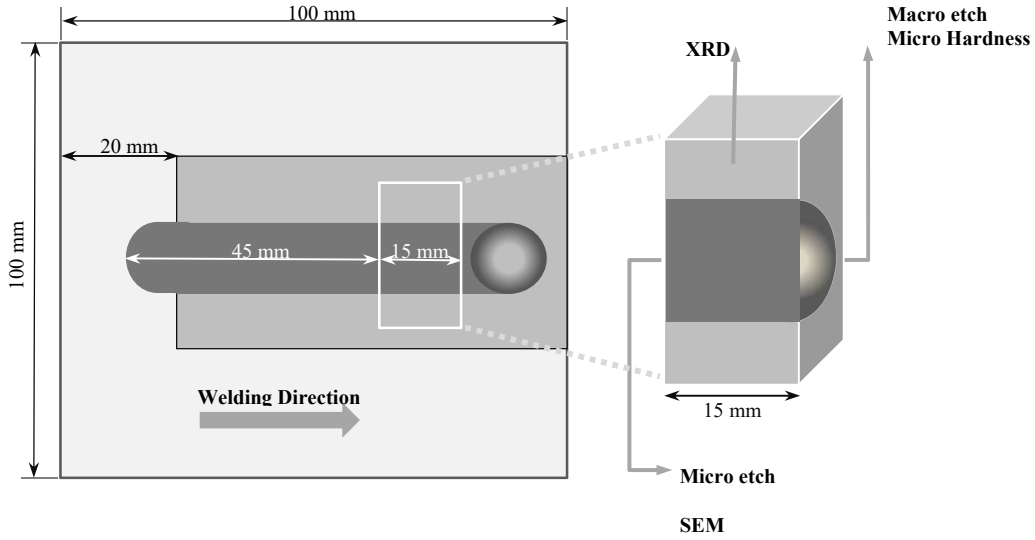

Fig. 1 Schematic view of tests piece locations on a flux coated sample

Weld cross sections were studied by optical and scanning electron microscopes. For optical macrography, all samples were first polished with grade 1000 abrasive paper, and then etched for 5 seconds in 0.5% HF solution. For micro etching, the surface polishing reapplied with grade 2500 abrasive paper and 0.05 μm alumina powder; then the surface was etched by rubbing on cotton for 10-20 seconds in Poulton solution. Optical microscope was used to observe micro etching results. SEM was performed using EDS (Energy Dispersive Spectroscopy) aided electron microscope. Vickers Microhardness measurement was also applied by 100 gf in 10 sec. Finally, X-Ray diffraction method was used to analyze the slag formed on the weld surface.

III. Results and Discussion

A. Arc Stability and Weld Bead Inspection

It was observed that the arcs are initiated with some seconds delay on the aluminum surface depending on the welding current. Increasing the heat input by raising the current, resulted in decreasing this duration. At the lowest current (105A) it took 18 seconds to form a stable arc and weld pool. By increasing the current to 175A this duration was decreased to 6 seconds. Using alternating current (AC) with just a half cycle electrode positive polarity for breaking the stable oxide film of aluminum produced a loud vibrating noise at the beginning which gradually reduced, and a relatively stable arc was obtained after formation of the weld pool. As the arc travelled to the flux coated area, this stability was disturbed due to electrical resistance of the solid oxide flux. This arc instability in AC-ATIG process has been also reported in other studies [12], [13], [22], [26].

Arc stability increased with decreasing the flux layer thickness and increasing the heat input. It can be explained by the fact that increasing the heat input simplifies melting of ZnO flux which modifies the electrical conductivity between arc and the metal. Presence of molten flux at the edges of the weld pool was observed as reported by Zhao et al. [28]. The plate surface below the arc had a seemingly concave form, specifically for samples with higher flux thickness, which is also supported by previous researchers' observations [12]-[14], [19].

Visual inspection of the reference TIG welds showed regular weld beads with a gradual width increase from the start to the end of the weld line. The reason can be high thermal conductivity of aluminum and the small size of plates, which results to fast increase in plates' temperature during welding. The first effect of using the flux seems to be an unfavorable visual feature of the weld bead. Presence of sticking slag had disturbed the arrangement of the weld beads, and only in some samples the central part of the weld metal surface was observable; and at the outer sides, the non-used flux remained as shown in Fig. 2. Each sample is assigned a code. As shown in Fig. 2, increasing flux thickness resulted in more and coarser slag particles that covered the whole weld bead. By raising the heat input, the width of the weld bead was increased.

B. Weld Geometry

Table III presents geometrical dimensions of the welds that were measured by graphical image screen calculation. Three parameters of depth to width ratio (D/W), relative weld penetration (D_{ATIG}/D_{TIG}), and relative weld section area (A_{ATIG}/A_{TIG}) were used to investigate the effect of using flux on the size and shape of weld pool.

At the lowest current (105A), while a 30% decrease of the relative penetration was observed for the flux thickness of 30 μm, a significant increase was seen for the flux thicknesses of 60 and 90 μm. This result can support the theory of flux activation due to a certain oxygen content in the weld metal. Studies have been conducted on effects of different oxygen contents in ATIG welds [20], [24], [28]. It can be inferred that for flux thickness of 30 μm (sample Zn11), the oxygen content of the weld is not high enough to trigger the activation mechanism; and that the starting point of the activation

mechanism occurs when the flux thickness is a value between 30 and 60 μm. The decrease in the D_{ATIG}/D_{TIG} parameter for Zn11 sample, can be explained by the energy loss due to melting of the flux particles.

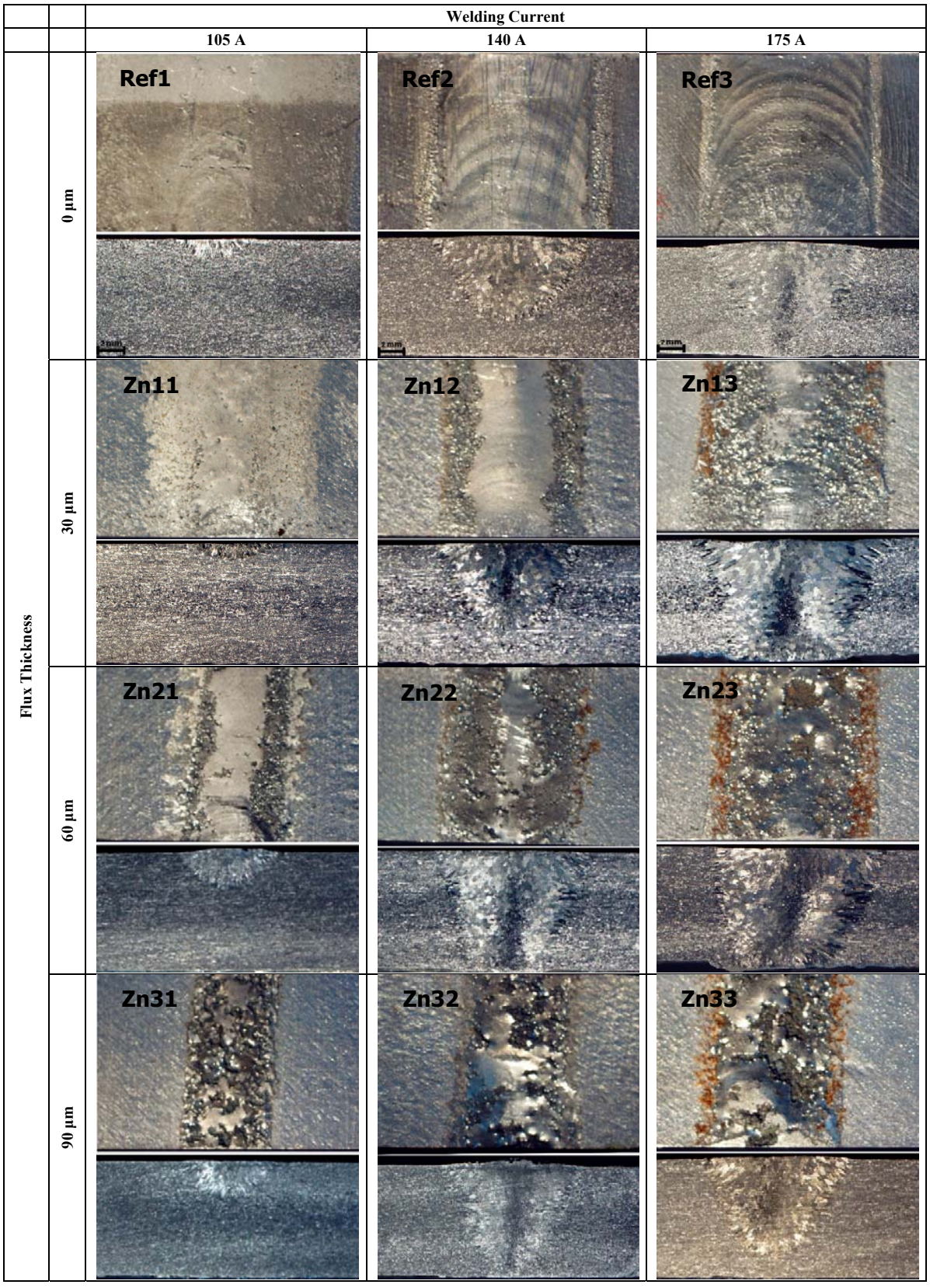

Fig. 2 Surface and cross sections of the welds after macro etching

TABLE III
GEOMETRICAL DIMENSIONS OF THE WELDS

Current	A	105				140				175			
Sample Code		Ref1	Zn11	Zn21	Zn31	Ref2	Zn12	Zn22	Zn32	Ref3	Zn13	Zn23	Zn33
Flux thickness	µm	0	30	60	90	0	30	60	90	0	30	60	90
Weld width (W)	mm	7	7.4	7.0	7.3	11.2	12	11.4	10.2	12.8	14.0	12.2	**11.0**
Weld depth (D)	mm	1.5	1.1	3.2	3.1	6.1	6.3	8.4	8.0	8.2	8.5	8.6	**6.9**
D / W	_	0.21	0.15	0.46	0.42	0.54	0.53	0.74	0.78	0.64	0.61	0.70	**0.63**
D_{ATIG}/D_{TIG}	_		0.7	2.1	2.1		1.0	1.4	1.3		1.0	1.0	**0.8**
A_{ATIG}/A_{TIG}	_		0.7	1.8	2.0		1.0	1.5	1.2		1.5	1.5	**0.8**

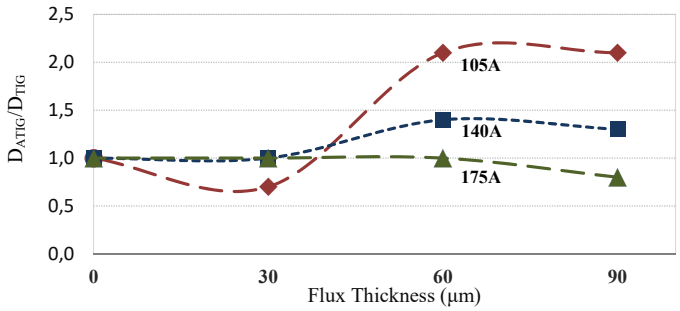

Fig. 3 Relative penetration depth versus flux layer thickness at different welding currents

By increasing the heat input to 145A, no significant increase in relative penetration was observed for higher flux thicknesses compared to 105A. Raising the current to 175A results in equal or less weld penetrations. It is concluded that weld penetration increase due to use of active flux is obtained at lower heat input values, and with increasing the welding current, no or negative increase in penetration depth occurs. This effect can be explained by the theory of several forces in the weld pool [42], [44], [13]. According to this theory, electromagnetic (Lorentz) force plays the main role at higher currents, while at lower currents the other forces, particularly surface tension force can be dominant. In this study, decrease of the relative penetration for 175A can be explained by spending more arc energy to melt the flux without any positive effect on increasing the weld depth. In fact, increase of penetration depth in aluminum, converts to increase of width and consequently volume of the weld, due to its high thermal diffusion and conduction coefficient.

Fig. 3 shows that the highest relative penetrations were obtained at the lowest current and the flux thicknesses above 60 µm (samples Zn21, Zn31). It has been also demonstrated by previous researchers that ATIG is more effective in lower currents compared to the TIG welds [1], [12], [19], [45]. In addition, it can be observed that the relative penetration initially improves with flux thickness increase and shows no significant increase or even a minor decrease for higher flux thicknesses. Similar pattern for relative penetration changes relative to flux thickness has been reported by previous researchers [19], [20], [24], [26]. This observed trend supports the theory that surface activating effect occurs for a specific range of activator concentration, which was also mentioned previously in the introduction part of the article. In this study, the highest value was obtained for the flux quantity of 60 µ or 34 mg/cm^2.

Comparing values of relative area parameter (A_{ATIG}/A_{TIG}) in Table III indicates that the weld pool size increases for ATIG welds with $D_{ATIG}/D_{TIG}>1$. Similar results have been observed by previous researchers [10], [13], [22], [27]. However, this value is reported unchanged in other studies [29]. The values for the parameter depth/width (D/W) expresses that most of this increase is in the depth direction. It can be concluded that arc efficiency is improved in ATIG processes due to melting more metal by the same current value.

C. Metallography of Weld Cross Sections

Macro-etching of the weld cross sections revealed grains and solidification structures. As shown in Fig. 4, three structural zones can be seen in weld area. Starting from the weld border to the center, the epitaxial grains at the outer zone are the result of initial high cooling rate, then the columnar grains of directional solidification steps in, and finally the internal equiaxed grains are formed as a result of the slow solidification rate. In some of the previous studies, a similar internal structure was referred to as stray grain zone [48] and coarse basaltic zone [49].

Width of each zone in different samples depends on heat input and weld pool size [48]. So, it can be due to the high cooling rate of the small weld pool, that equiaxed structure zone is not observed in samples of 105A current. Microstructure of a pure aluminum consists of a bright α-Al matrix and a number of darker particles distributed in the matrix. Because of similarity of the grains structure, the grain boundaries may not be clearly observed by usual etching processes. Fig. 5 (a) shows such a structure in the HAZ. In larger weld pools the boundaries are clearer due to receipt of more heat. In Fig. 5 (b), the columnar structure is observed in the fusion boundary zone (FZ). Some of the previous researchers [6], [49]-[51] reported similar structures in partially melted zone (PMZ) which is a narrow zone outside

the FZ with a columnar structure, but with different composition along grain boundary.

In the weld center, the equiaxed grains can be seen (Fig. 5 (c)). The dark particles can be Al-Si eutectic phase or Al_3Fe intermetallic compound according to the chemical analysis of the alloy and binary phase diagrams. Similar solidification structure patterns also have been reported in previous TIG welding studies of the aluminum alloys [8], [52].

No significant difference in microstructure was observed between ATIG and TIG samples, as reported by some of the previous researchers [40], [17].

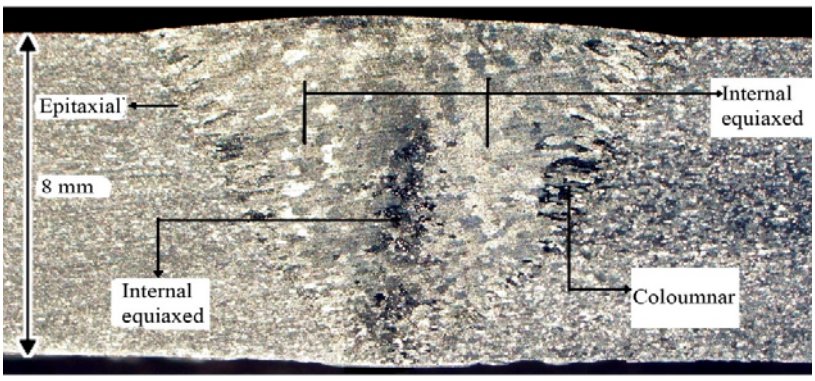

Fig. 4 Solidification structure of different zones in the cross section of sample Ref3

SEM on the same section of microstructures determined the composition and morphology of the particles. Fig. 6 presents the SEM images taken from two samples; and Table IV shows the chemical analysis results from EDS. Dark spaces that appear to be aligned can be grain boundaries. EDS revealed that most of these grain boundaries are only composed of aluminum. Scanning the lighter zones around these spots determined small quantities of Fe (point 3 in Fig. 6 (b)); and the brighter, larger particles among them are mainly Al-Si (points 1 and 2 in Fig. 6 (a)). There were also a very limited number of particles that contain three elements of Al, Si and Fe. This pattern of particle distribution was quite similar for all samples and no significant differences were observed between ATIG and TIG welds. Similar particles distribution in the α-Al matrix has been observed for different alloys composition by previous researchers [2], [6], [7], [53], [54].

It is notable that scanning for zinc, even near the surface of the welds did not reveal any quantities of this element. This observation demonstrated that the flux has no effect on chemical composition of the base metal during the ATIG process.

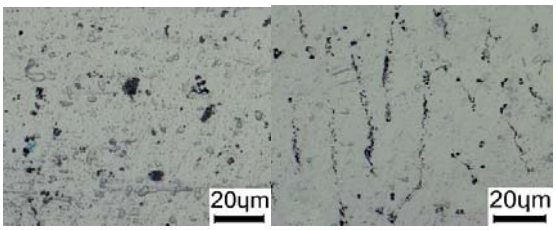

(a) (b)

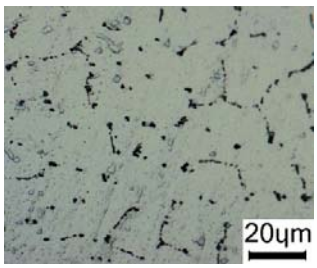

(c)

Fig. 5 Microstructures of the weld cross section of sample Zn23 HAZ (a), FZ (b), Weld metal (c)

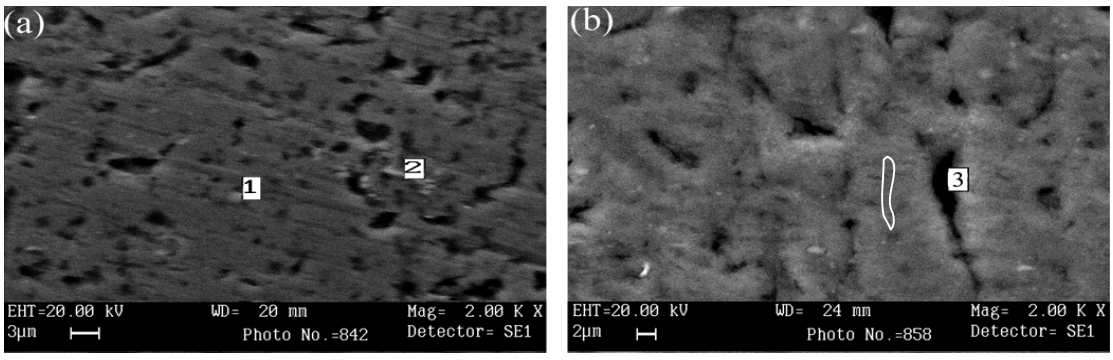

Fig. 6 SEM images of samples Zn13 (a) and Zn23 (b) x2000

TABLE IV
CHEMICAL ANALYSIS BY EDS AT POINTS OF FIG. 6

Point	Sample-location	Al%	Si%	Fe%
1	Zn13 – HAZ	77.61	22.39	_
2	Zn13 – HAZ	38.34	61.66	_
3	Zn23 – WM	99.32	_	0.68

D. X-Ray Diffraction Pattern of the Slag

X-Ray diffraction analysis was carried out to study the slag composition for the sample Zn33. In Fig. 7, the major peaks of diffraction pattern for this sample, determine the Al element. The same results have been reported by previous researchers [12]. Observing more than three peaks of ZnO, confirms it as another major compound. In addition, presence of some weak peaks of $Al_{2.4}Zn_{0.3}O_4$ compound demonstrates chemical reactions between the flux and the base metal. Presence of the slag at the central zone of the weld surface can be resulted from convergent flow of the melt in the weld pool. These observations are compatible with the theory of inversing Marangoni convection in ATIG welding [42].

E. Microhardness

Hardness measurements on weld samples cross sections at 140A, demonstrated the hardness profiles of Fig. 8. The hardness profile patterns for all samples are similar, as shown in Fig. 8. Hardness decreases with moving from the weld center to the HAZ, and then on the base metal it returns to its approximate value at the weld center. This hardness loss in the HAZ is expected. Hardness decrease occurs in a metal that has been previously under heat treatment or cold work, as a result of recrystallization in the HAZ [34], [55], [2]. This softening takes place even in solid state joining (i.e. friction stir welding - FSW) of Al-Alloys which are cold rolled prior to joining [56].

Equal values of hardness at the center and the base metal can be attributed to the purity of base metal and weld center equiaxed grain structure. Hardness values for both the reference TIG and the ATIG welds were in a same range. Nagraj [11] and Vora et al. [40] reported no change in hardness in ATIG welds compared to TIG.

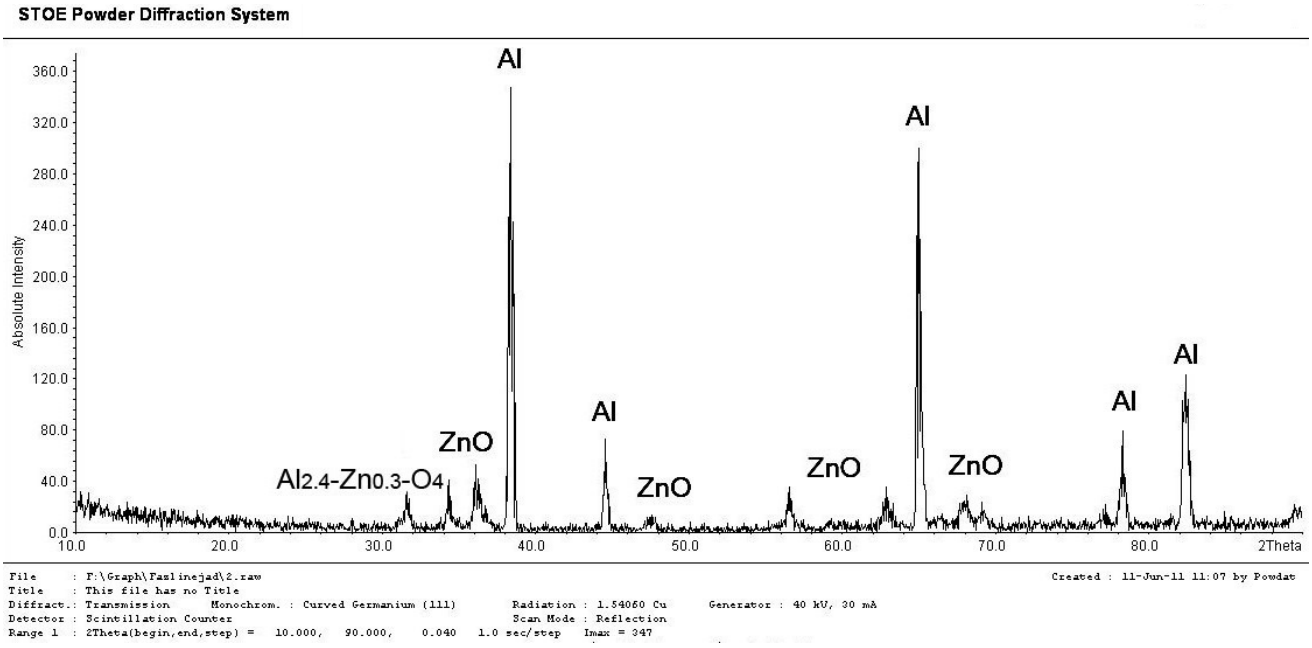

Fig. 7 Intensity-2θdiagram resulted from the XRD of sample Zn33

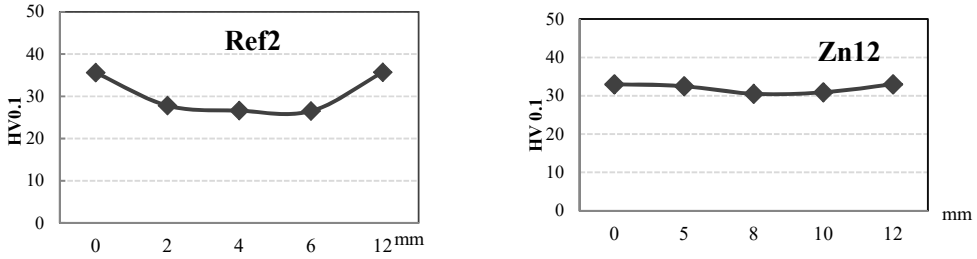

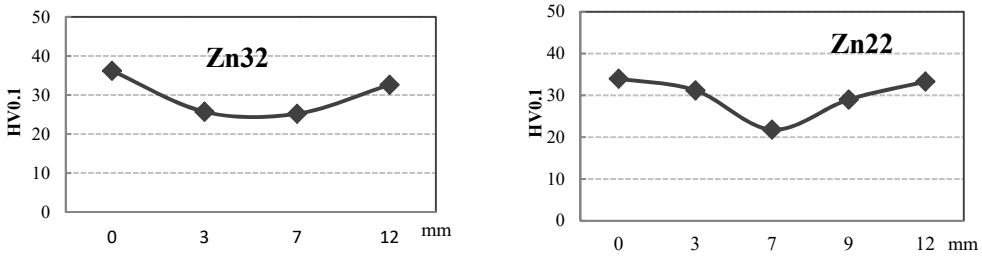

Fig. 8 Micro Hardness profiles for samples welded at 140 A current

IV. Conclusions

In this research, the properties of AC - ATIG process with ZnO flux on 1050 aluminum plates was studied and was compared with those of TIG welds. The main results are indicated below:

I. ZnO can perform as an active flux within a specified range of heat input and flux layer thickness in pure aluminum welding. In this study, samples welded at 105A current with 60 and 90µm flux thicknesses demonstrated 2.1time higher value of penetration depth compared to the TIG welds. In addition, increase of the depth to width ratio (D/W) and the weld pool size were observed in those samples of ATIG welds that showed an increase in penetration depth.

II. It was observed that ATIG is more effective in lower currents compared to the TIG. Values for relative penetration of ATIG to TIG welds illustrated that with increasing heat input, flux activation effect decreases.

III. In both TIG and ATIG welds, Metallographic images revealed epitaxial, columnar, and equiaxed grain zones. Minor presence of Al-Si and Al-Fe particles detected by SEM-EDS. Zinc as an element or in a compound state was not detected in the weld metal, which reveals that the flux has no effect on chemical composition of the base metal in ATIG.

IV. A sticking porous slag remained after welding and the weld bead appearance was not favorable. Applying XRD on the slag demonstrated that the slag composition is Al, ZnO and a compound with $Al_{2.4}Zn_{0.3}O_4$ stochiometric formula.

V. Hardness profiles showed a decrease in the HAZ compared to the weld center and the base metal. No significant differences were observed between TIG and ATIG welds.

VI. Arc initiation and traveling on the flux coated surface of aluminum was difficult and seemed unstable compared to the conventional TIG. In order to use the discussed ATIG process in mass production, its' drawbacks, including flux coating cost, sticking slag formation on the surface, unfavorable visual weld bead, and implementation difficulties, should be considered. On the other hand, the ATIG process compared to TIG is associated with some advantages including higher penetration depth which results in higher production rate. In addition, it requires lower welding current, smaller HAZ and less distortion due to less required number of weld runs.

References

[1] Li M., Shengsun H., Bao H., Junqi S., Yonghui W., "Activating Flux Design for Laser Welding of Ferritic Stainless Steel ", Trans. Tianjin Univ. 2014, 20, 429-434.

[2] Pakdil M., Çam G., Koçak M., Erim S., "Microstructural and mechanical characterization of laser beam welded AA6056", Mater. Sci. and Eng., 2011, 528(24), 7350– 7356

[3] Cam G., Ventzke V., Dos Santos J. F., Kocak M., Jennequin G., and Gonthier-Maurin P., "Characterisation of electron beam welded aluminum alloy", Scie. and Tech. of Weld. Join., 1999, 4(5), 317-323.

[4] Dey, V., Pratihar, D. K., Datta, G. L., Jha, M. N., Saha, T. K., and Bapat, A. V., "Optimization and prediction of weldment profile in bead-on-plate welding of Al-1100 plates using electron beam ", Int. J Adv. Manuf. Tech., 2010, 48, 513–528.

[5] Sibillano T., Ancona A.; Berardi V.; Schingaro E.; Basile G.; Mario Lugarà P., "A study of the shielding gas influence on the laser beam welding of AA5083 aluminium alloys by in-process spectroscopic investigation", Opt. Las. Eng., 2006, 44, 1039-1051.

[6] Zhao Y.B., Lei Z.L., Chen Y.B., Tao W, "A comparative study of laser-arc double-sided welding and double-sided arc welding of 6 mm 5A06 aluminum alloy", Mater. Des., 2011, 32(4), 2165–2171.

[7] Hirose A., Todaka H., and Kobayashi KF, "CO2 Laser Beam Welding of 6061-T6 Aluminum Alloy Thin Plate", Metall. Mater. Trans A, 1997, 28(12), 2657-2662.

[8] Çam G., Koçak M., Progress in joining of advanced materials: part 1: solid state joining, fusion joining, and joining of intermetallics, Sci. Techno. Weld. Goin., 1998, 3(3), 105-126, Taylor & Francis.

[9] Cam G., Ventzke V., Dos Santos J. F., Kocak M., Jennequin G., Gonthier-Maurin P., Penasa M., Rivela C., Boisselier D., "Characterization of laser and electron beam welded Al alloys", Prakt. Metallorg., 1999, 36(2), 59-89.

[10] Shyu S.W., Huang H. Y., Tseng K. H. and Chou C. P. "Study of the performance of stainless steel A-TIG welds", J. Mater. Eng. and Perform, 2008, 17, 193-201.

[11] Niagaj J., "The use of activating fluxes for the welding of high-alloy steels by A-TIG method" Weld. Int., 2003, 17(4), 257-261.

[12] Qing-ming L., Hong W. X., Zeng Z., Jun W, "Effect of activating flux on arc shape and arc voltage in tungsten inert gas welding", Trans. Nonferrous Met. Soc. Chi., 2007, 17, 486- 490.

[13] Sire S., Marya S., "On the selective silica application to improve welding performance of the tungsten arc process for a plain carbon steel and for aluminum", C. R. Mecanique, 2002, 330(2), 83–89.

[14] Huang Y., Fand D., Fan Q., "Study of mechanism of activating flux increasing weld penetration of AC A-TIG welding for aluminum alloy", Front. Mech. Eng. Chi., 2007, 2(4), 442–447.

[15] Dey, H. C., Albert, S. K., Bhaduri, A. K., Kamachi Mudali, "Activated flux TIG welding of titanium Weld", World, 2013, 57(6), 903-912.

[16] Jayakrishnan S., Chakravarthy P., Muhammed Rijas A., "Effect of Flux Gap and Particle Size on the Depth of Penetration in FBTIG Welding of Aluminum", Trans. Indian Inst. Met., 2016,1-7

[17] Liu G., Liu M., Yi Y., Zhang Y., Lou Y., Xu L., "Activated flux tungsten inert gas welding of 8 mm-thick AISI 304 austenitic stainless steel", J. Cent. South Univ., 2015, 22(3), 800-805.

[18] Prilutsky V. P., Akhonin S. V., "TIG welding of titanium alloys using fluxes", Weld. World, 2014, 58(2), 245-251.

[19] Ramkumar, K. D., Varma, J. L. N., Chaitanya, G. et al., "Experimental investigations on the SiO2 flux-assisted GTA welding of super-austenitic stainless steels", Int. J. Adv. Manu. Tech., 2015, 1-12.

[20] Ahmadi E., Ebrahimi A. R., "Welding of 316L Austenitic Stainless Steel with Activated Tungsten Inert Gas Process", J. Mater. Eng. Perf., 2015,

24, 1065–1071.
[21] Santhana Babu A. V. Giridharan P. K., "Productivity improvement in flux assisted TIG welding", Int. J. des. Manu. Tech., 6(2), 2012, 55-62.
[22] *Zhang Z*., *Liu L*., Sun H., Wang L., "AC TIG welding with single-component oxide activating flux for AZ31B magnesium alloys", J Mater Sci., 2008, 43, 1382–1388.
[23] Bonnefois B., Coudreuse L., Charles J., "A-TIG welding of high nitrogen alloyed stainless steels: a metallurgically high-performance welding process", Weld. Int., 2004, 18(3) 208-212.
[24] Lu Sh., Fuji H., Sugiyama H. and Nogi K., "Mechanism and optimization of oxide fluxes for deep penetration in gas tungsten arc welding", Metal. Mater. Trans. A, 2003, 34(9), 1901-1907.
[25] Modenesi P. J., Apolinário E. R., Pereira I. M., "TIG welding with single-component fluxes", J. Mater. Process. Tech., 2000, 99, 260-265.
[26] Ru¨ckert G., Huneau B., Marya S., "Optimizing the design of silica coating for productivity gains during the TIG welding of 304L stainless steel", Mater. Des. 2007, *28*, 2387–2393.
[27] Huang H. Y., "Effects of shielding gas composition and activating flux on GTAW weldments", Mater. Des., 2009, 30, 2404–2409.
[28] Zhao, Y., Shi, Y. & Lei, Y., "The Study of Surface-Active Element Oxygen on Flow Patterns and Penetration in A-TIG Welding", Metall. and Mater. Trans. B 2006, 37(3), 485-493
[29] Huang H. Y., "Effects of activating flux on the welded joint characteristics in gas metal arc welding", Mater. Design, 31, 2010, 2488–2495.
[30] Zhang R., Fan d., Katayama S., "Electron beam welding with activating flux", Trans. JWRI, 2006, 35(2), 19-22.
[31] Perumal K., Vivek N., Venkataaramanan M. S., Gurubalaji R., "Experimental investigation on TIG welded of austenitic stainless steel L304", Int. J. Sci. Eng. Res., 7(2), 2016, 123-129.
[32] Paniagua-Mercado A. M., López-Hirata V. M., Méndez-Sánchez A. F., Saucedo-Muñoz M. L., "Effect of Active and Nonactive Fluxes on the Mechanical Properties and Microstructure in Submerged-Arc Welds of A-36 Steel Plates", Mater. Manu. Proc., 22(3), 295-297.
[33] Richetti A., Silva H. D., Groetelaars PJ., Oliveira O. M., "Application of Flux Prepared way in welding plasma with keyhole", 13th POSMEC – Symp. Grad. Prog. in Mech. Eng.
[34] Mathers G., "The welding of aluminum and its alloys", First published 2002, Woodhead Publishing Ltd', Ch.2, 16-32.
[35] Dhandha K. H, Badheka V. J., "Effect of activating fluxes on weld bead morphology of P91 steel bead-on-plate welds by flux assisted tungsten inert gas welding process", J. Manu. Proc., 2015, 17, 48–57.
[36] Huang H. Y., Shyu S. W., Tseng K. H., Chou C. P., "Evaluation of TIG flux welding on the characteristics of stainless steel", Scie. Tech. Weld. Join., 2005, 10(5), 566-573.
[37] Choudhary S., Duhan R., "Effect of Activated Flux on Properties of SS 304 Using TIG Welding", Int. J. Engineering Trans. B: Apps., 2015, 28(2), 290-295.
[38] Kumar, SA; Sathiya, P., "Experimental Investigation of the A-TIG Welding Process of Incoloy 800H", Mater. Manu. Proc., 2015, 30(9), 1154-1159.
[39] Zhang Z., Fan F., Wang J., Liu L., 'Effects of Oxide on Plasma in Arc Welding With Activating Fluxes', IEEE Trans. Plasma Sci., 2014, 43, 465-471.
[40] Vora J. J., Badheka V. J., "Improved Penetration with the Use of Oxide Fluxes in Activated TIG Welding of Low Activation Ferritic /Martensitic Steel", Trans. Indian Inst. Met., 2016, 69(9), 1755–1764.
[41] Bang, K.-S. Chirieleison G., Liu S., "Gas tungsten arc welding of titanium using flux cored wire with magnesium fluoride", Sci. Tech. Weld. Join., 2005, 10(5), 617-623.
[42] Kou S., "Welding metallurgy', 2nd edition., John Wiley & Sons, Inc., New Jersey, 2003, Ch. 4.2.
[43] Limmaneevichitr C., Kou S., "Experiments to Simulate Effect of Marangoni Convection on Weld Pool Shape", Weld. J., 2000, 79(8), 231-237.
[44] Yushchenko K. A., Kovalenko, D. V., Krivtsun I. V., Demchenko V. F., Kovalenko I. V., Lesnoy A. B., "Experimental Studies and Mathematical Modelling of Penetration in TIG and A-TIG Stationary Arc Welding of Stainless Steel", Weld. World, 2009, 53(9), 253-263.
[45] Heiple, C. R., and Roper, J. R, "Mechanism for minor element effect on GTA fusion zone geometry", Weld. J., 1982, 61(4), 97-102.
[46] Limmaneevichitr C., Kou S., "Visualization of Marangoni Convection in Simulated Weld Pools", Weld. J., 2000, 79(5), 126–135.
[47] Leconte S., Paillard P., Chapelle P., Henrion G., Saindrenan J., "Effect of oxide fluxes on activation mechanisms of tungsten inert gas process", Scie. Tech. Weld. Join.,11(4), 2006 - 389-397.
[48] Arata Y., Matsuda F., Matsui A., "Effect of Welding Condition on Solidification Structure in Weld Metal of Aluminum AIloy Sheets", Trans. JWRI, 1974, 3(1), 89-97.
[49] Karalis D. G., Pantelis D. I., Papazoglou V. J., "On the investigation of 7075 aluminum alloy welding using concentrated solar energy", Solar Ener. Mater. Solar Cells, 2005, 86(2),145–163.
[50] Prasad Rao K., Ramanaiah N., Viswanathan N., "Partially melted zone cracking in AA6061 welds", Mater. Des., 2008, 29,179–186.
[51] Huang C., Kou S., "Partially Melted Zone in Aluminum Welds — Liquation Mechanism and Directional Solidification", Weld. J, 2000, 113-120.
[52] Manti R., Dwivedi D. K., Agarwal A, "Pulse TIG Welding of Two Al-Mg-Si Alloy", J. Mater. Eng. Perf., 2008, 17(5), 667–673.
[53] Norman A. F., Drazhner V., Prangnell P. B, "Effect of welding parameters on the solidification microstructure of autogenous TIG welds in an Al–Cu–Mg–Mn alloy", Materials Science and Engineering A259, 1999, 259(1), 53–64.
[54] Monteiro VM., Diniz SB., Meirelles BG., Da Silva LC., Dos Santos Paula A., Microstructural and mechanical study of aluminum alloys submitted to distinct soaking times during solution heat treatment', Tec. Metal. Mater. Miner., 2014, São Paulo, 11(4), 332-339.
[55] Çam G., Güçlüer S., Çakan A., Serindag H. T., "Mechanical properties of friction stir butt-welded Al-5086 H32 plate", Mat.-wiss. u. Werkstofftech., 2009, 40(8), 638–642.
[56] Çam G., Mistikoglu S., "Recent developments in friction stir welding of Al-alloys treatment", J. Mater. Eng. Perf. (JMEPEG), 2014, 23(6),1936-1953.